The Thesis Committee for Joshua Abel Leibowitz
Certifies that this is the approved version of the following thesis:

TIN-BASED NANOCOMPOSITE ALLOY ANODES FOR LITHIUM-ION BATTERIES

APPROVED BY
SUPERVISING COMMITTEE:

Supervisor:

Arumugam Manthiram

Guihua Yu

TIN-BASED NANOCOMPOSITE ALLOY ANODES FOR LITHIUM-ION BATTERIES

by

Joshua Abel Leibowitz, B.S.E.

Thesis

Presented to the Faculty of the Graduate School of

The University of Texas at Austin

in Partial Fulfillment

of the Requirements

for the Degree of

Master of Science in Engineering

The University of Texas at Austin

May 2014

Acknowledgements

I would like to thank my advisor, Professor Arumugam Manthiram for allowing me to perform research in his group and giving me guidance. I would also like to thank Prof. Guihua Yu for being my thesis reader.

I would like to thank Eric Allcorn for helping me to start out in the lab, and for his input on revisions of papers and general research. I would also like to thank Sang Ok Kim and Il Tae Kim for working with me in the anodes subgroup, and Longjun Li for helping me take HRTEM images and diffraction patterns.

Abstract

TIN-BASED NANOCOMPOSITE ALLOY ANODES FOR LITHIUM-ION BATTERIES

Joshua Abel Leibowitz M.S.E.

The University of Texas at Austin, 2014

Supervisor: Arumugam Manthiram

Lithium-alloying anode materials have attracted much attention as an alternative to carbon due to their high theoretical gravimetric capacities (e.g. $Li_{4.4}Si$: 4200 mAh g^{-1}, $Li_{4.4}Sn$: 990 mAh g^{-1}, and Li_3Sb: 660 mAh g^{-1}). An additional benefit of lithium alloying metals is that some of the react at a higher potentials vs. Li/Li^+ than carbon, which can mitigate safety issues caused by solid-electrolyte interface layer formation and lithium plating. One of the most promising lithium -alloying anode materials that are being pursued are Sn-based materials due to their high capacity and tap density.

This thesis investigates the synthesis and characterization of Sn-based lithium-ion battery anodes. SnSb-TiC-C and $FeSn_2$-TiC nanocomposite alloy anodes for lithium-ion batteries have been synthesized by a mechanochemical process involving high-energy mechanical milling of Ti/Sn, Ti/M (M = Fe or Sb), and C. Characterization of the nanocomposites formed with x-ray diffraction (XRD), scanning electron microscopy

(SEM), and transmission electron microscopy (TEM) reveals that these alloys are composed of crystalline nanoparticles of $FeSn_2$ and SnSb dispersed in a matrix of TiC and carbon. The SnSb-TiC-C alloy shows an initial gravimetric capacity of 653 mAh g-1 (1384 mAh cm^{-3}), an initial coulombic efficiency of 85%, and a tap density of 1.8 g cm^{-3}. The $FeSn_2$-TiC alloy shows an initial gravimetric capacity of 510 mAh g^{-1} (1073 mAh cm^{-3}), an initial coulombic efficiency of 71%, and a tap density of 2.1 g cm^{-3}. The TiC-C buffer matrix in the nanocomposite alloy anodes accommodates the large volume change occurring during the charge-discharge process and leads to good cyclability compared to pure $FeSn_2$ and SnSb anodes.

Table of Contents

List of Figures

Chapter 1: Introduction

1.1 Lithium-ion Battery Fundamentals

Due to their high energy density, lithium ion batteries have become ubiquitous as a power source for portable electronics and consumer devices. Lithium-ion batteries are also being pursued as power sources for electric vehicles (EV) and hybrid electric vehicles (HEV). Because of their high energy density compared to that of lead-acid, nickel-cadmium, and nickel-metal hydride batteries, lack of memory effect, and slow charge loss when not in use, lithium-ion batteries have come to dominate the rechargeable battery market. Often, for portable devices and EV and HEV, volumetric capacity and volumetric energy density are more important than gravimetric capacity, due to the need to conserve space in designs. In addition to energy density and capacity, other important factors to control in lithium-ion batteries are the charge rate, cycle life, and safety.[1]

A typical lithium-ion battery consists of a negative and positive electrode (anode and cathode) separated by an electrolyte, typically a porous membrane, which facilitates the flow of ions. When a lithium-ion battery is discharged, lithium ions are extracted from the anode, flow through the electrolyte and separator membrane, and become inserted into the cathode host matrix. The reverse process occurs when a lithium-ion battery is charged. This process should be as reversible as possible, with the host matrix maintaining its structure during lithiation and delithiation. The open-circuit voltage of a

lithium ion battery can be obtained from the difference in the lithium chemical potential between the cathode ($\mu_{(Li(c))}$) and the anode ($\mu_{(Li(c))}$), which is given by the equation:[2]

$$VOC=\mu Li(c)-\mu Li(a)F \quad (1)$$

where F is the Faraday's constant. The cathode and anode must also be chosen so that they lie within the band gap of the electrolyte, to prevent oxidation or reduction of the electrolyte during lithiation/delithiation.

1.2 THE NEED FOR NEW ANODE MATERIALS

Lithium-alloying anode materials have attracted much attention due to their high theoretical gravimetric capacities (e.g. $Li_{4.4}Si$: 4200 mAh g^{-1}, $Li_{4.4}Sn$: 990 mAh g^{-1}, and Li_3Sb: 660 mAh g^{-1})[3]. An additional benefit of lithium alloying metals is that some of them react at a higher potential vs. Li/Li^+ than carbon, which can reduce the formation of a solid-electrolyte interface (SEI) layer. SEI layer formation can lead to of significant irreversible capacity in the first cycle, and lowered charge rate.[2,4] In addition, a higher reaction potential can prevent lithium plating on the electrode surface and eliminate or minimize to dendrite growth and safety concerns.[5] One of the most promising lithium-alloying anode materials that has been pursued is Sn-based materials due to their high capacity, tap density, and their higher potential vs. Li/Li^+ .[6-8] The most significant issue with Sn-based alloy anodes such as Cu_6Sn_5 or $FeSn_2$ is the large volume change that occurs during the lithiation and delithiation processes. This volume change results in lattice stress and crumbling of active electrode particles, which leads to rapid capacity

fade.[9-11] Some methods which have been attempted to mitigate the negative effects of volume change are reducing the active Sn to nanoscale particles, incorporating a reinforcing matrix around the active material, and alloying the active material with an inactive buffer material. This thesis describes a synthesis procedure that combines all three of the above strategies, creating nanostructured Sn-based composites with a TiC-based reinforcing matrix.

1.3 Improving the Properties of Alloy Anode Materials

While lithium-alloying anode materials are an ideal alternative to graphite due to their high capacities and cyclability, something must be done to mitigate their downsides, such as the aforementioned issues caused by volume change and particle agglomeration. One method that is often attempted to improve upon this is to reduce the particle size into the microscopic or nanoscopic regime, often through chemical synthesis such as reduction reactions, or through high energy mechanical milling (HEMM). Reduction of particle size improves the cycle life of alloy anodes by reducing the internal strains, minimizing the damage occurring due to volume expansion. In addition, this serves to lower the diffusion lengths necessary for lithium during the lithiation/delithiation process.[12-13] Increasing the surface to volume ratio by reducing the particle size does increase the amount of surface reactions with the electrolyte, however, which can lead to further safety issues.

One alternate method for improving alloy anode cycle life is the creation of a nonreactive reinforcing matrix such as Al_2O_3 or TiC. Such a matrix surrounding the

active material particles can act as a buffer for volume expansion, preventing particle crumbling and reducing the effects of internal stresses.[14-16] A buffer matrix can also serve to prevent particle agglomeration. Many times, carbon is incorporated into an alloy anode as a matrix material, to provide conductivity and additional capacity while also providing a buffer for internal stresses.[14-18]

A similar method for improving the cycle life of alloy anode materials is to create active-inactive composite materials. This consists of the active material (often Si, Sn, or Sb) alloying or mixing with an inactive metal which will serve as a buffer matrix. The inactive-active material alloy can react with lithium either in a conversion reaction or in an addition reaction. A conversion reaction, such as NiSb or $FeSn_2$, proceeds by extruding the inactive component to form an inactive buffer matrix, while the active component (Sb or Sn in these cases) reacts with lithium.[19-20] An addition reaction, such as Cu_2Sb or $FeSb_2$ incorporates lithium into the material to form a ternary phase, such as Li_2CuSb. In both of these cases, the inactive material serves to dampen the effects of strain due to volume change. Dahn *et al*[21] have investigated several Sn-M-C systems, including those where M = Ti, V, Cr, Mn, Fe, Co, Ni, and Cu. $FeSn_2$ in particular was reported to have a specific capacity of 650 mAh/g.[22] Many other studies have been carried out on active-inactive composites, most of which have seen a significant enhancement in cycle life and reversibility of anodes, though they do come with a tradeoff of lowered capacity

Some of the most promising lithium-alloying anode materials that have been suggested are Sn-based materials, which are ideal due to their high capacity ($Li_{4.4}Sn$: 990

mAh g^{-1}), tap density, and their higher potential vs. Li/Li^+. However, Sn-based materials suffer from the same issues that plague all intermetallic alloy anodes, namely those of capacity fade due to crumbling of the alloy after repeated cycling. Some papers have recently been published regarding nanocomposites of Sn-TiC-C[15] and Cu_6Sn_5-TiC-C[14] synthesized utilizing a high-energy mechanical milling (HEMM) method. The Sn-TiC-C composite and Cu_6Sn_5-TiC-C composites displayed stable cycling for 300 and 70 cycles, respectively, with specific capacities of 370 mAh g^{-1} and 570 mAh/g when cycled at 0 - 2 V. These composites showed significant improvement over previous Sn-based alloy anodes. In addition, they offered a compelling alternative to Sony's nexelion battery, which utilized a Sn-Co-C material, as cobalt is both expensive and toxic. The TiC-C served as a buffer matrix to the Sn, which was lithiated and delithiated during cycling. In the case of Cu_6Sn_5-TiC-C, the Cu was extracted and provided a buffer matrix as well, with the material transitioning from Cu_6Sn_5 to Li_2CuSn to $Li_{4.4}Sn$. Most of the irreversibility occurred during the transition from Cu_6Sn_5 to Li_2CuSn, so the cell performed more reversibly when cycled from 200 mV to 2 V, which is above the Cu_6Sn_5 to Li_2CuSn transition.

Building on the research carried out in our group, two nanocomposite alloy anodes have been synthesized in this thesis with $FeSn_2$-TiC and SnSb-TiC-C, with the goal of achieving high capacities and extended cycle life, utilizing cost-effective, nontoxic materials.

The active materials described in this thesis, SnSb and $FeSn_2$, are Sn-based intermetallics that react with lithium via a conversion reaction. In a conversion reaction,

the active materials are extruded from the alloy and interact with lithium. The reaction of SnSb with Li occurs in a two-step process as below:

$$SnSb + 3Li^+ + 3e^- \rightarrow Li_3Sb + Sn \quad (2)$$

$$Li_3Sb + Sn + 4.25Li^+ + 4.25e^- \rightarrow Li_3Sb + Li_{17}Sn_4 \quad (3)$$

The Sb reacts first, as it has a higher reaction potential of ~ 0.9 V vs. Li/Li^+. The reaction of Sn occurs in a second step at potentials of ~ 0.2 – 0.4 V and ~ 0.7 V vs. Li/Li^+:[23-26]

The reported reaction method for $FeSn_2$ is also a conversion reaction, though the Fe is extruded to form an inactive matrix rather than being lithiated and delithiated along with the Sn. The reaction of FeSn2 with Li occurs as below:[22,27]

$$FeSn_2 + 8.8Li^+ + 8.8e^- \rightarrow 2Li_{4.4}Sn + Fe \quad (4)$$

$$Li_{4.4}Sn \leftrightarrow Sn + 4.4Li^+ + 4.4e^- \quad (5)$$

While alloying Sn and other active intermetallics can help mitigate stresses caused by cycling, anodes made of bulk active alloys such as SnSb[23], $FeSn_2$[27], Cu_6Sn_5[17], or AgSn[28] still have difficulty achieving stable cycle performance. Improvements can be made by creating nanostructured materials, which have a larger surface area to volume ratio, shorter diffusion lengths for lithium ions, and can handle expansion and contraction while minimizing the buildup of internal stresses.[12-13] These nanoparticles can be incorporated into a composite with a reinforcing matrix such as TiC, Al_2O_3, or C, which could absorb some of these internal stresses and prevent breakdown of the active material.[14-18] Reinforcing matrices also prevent particle agglomeration during cycling.[29] The materials synthesized in this work utilize a reinforcing matrix of TiC, and are prepared by heating binary precursors composed of Ti/Sn and Ti/M (where M is Fe or Sb

for, respectively, the $FeSn_2$-TiC and SnSb-TiC-C based electrode powders). While $FeSn_2$ has a high capacity, it also has a relatively low initial coulombic efficiency when synthesized, meaning that a large amount of the capacity is lost during the first cycle. This corresponds to irretrievable lithium, which significantly limits the overall capacity of a full cell during subsequent cycles. A large first cycle coulombic efficiency is an important trait for an anode material to have, and if an intermetallic alloy anode can have a larger coulombic efficiency than natural graphite (76.2%),[30] it would be a promising alternative. $FeSn_2$-C was studied fairly extensively by Mao and Dahn, who found the best reversibility to occur with 25% active phase and 75% inactive phase ($SnFe_3C$), when Sn, Fe, and C were combined through HEMM.[22] In chapter 3, we will present the investigation of a $FeSn_2$-TiC nanocomposite synthesized through HEMM showing an initial gravimetric capacity of 510 mAh g^{-1} (mAh cm^{-3}), an initial coulombic efficiency of 71%, and a tap density of 2.1 g cm^{-3}.

SnSb has been a well-studied alloy anode material, due to the fact that it is composed of two commonly used intermetallics which actively react with lithium. SnSb/C nanocomposite materials were synthesized by Park and Sohn, with an initial coulombic efficiency of 81%, but no data was given on mass loading or tap density.[31] A SnSb-TiC-C nanocomposite synthesized via HEMM will be described in Chapter 3 with an initial gravimetric capacity of 653 mAh g^{-1} (1384 mAh cm^{-3}), an initial coulombic efficiency of 85%, and a tap density of 1.8 g cm^{-3}.

1.4 Synthesis Via High Energy Mechanical Milling (HEMM)

High energy mechanical milling is a materials synthesis method, which has traditionally been used for blending powders or crushing rocks. It is a type of ball milling where reactant materials are ground by balls within a cylinder at high speeds with a large amount of kinetic energy, operating similarly to a rock tumbler. The mechanical mill used in this work was a planetary ball miller, in which at least one grinding vial is arranged on a "sun wheel", away from the center. The "sun wheel" is rotated, and the balls within the jar are subjected to coriolis forces, with the difference in speed between the balls and grinding jars causing frictional and impact forces.[32] In the 1980s in a paper by Koch et al., it was discovered that mechanical milling can facilitate alloying of powders.[33] Mechanochemical synthesis via high energy mechanical milling is most likely to occur when the reactants have a thermodynamic driving force to be alloyed into compounds or solid solutions, such as a negative heat of mixing. If there is a thermodynamic driving force for an amorphous phase to form, then the only other factor determining whether a phase will form is the kinetic factor, which is related to the difficulty of nucleating the intermetallic compounds, and the environmental conditions within the mill. High energy mechanical milling is a preferred technique because it is cheap, easily scalable, and consistent. However, if the driving force for mechanochemical synthesis of a material is too high, there can be concern of a thermal runaway reaction when scaling to large amounts of powder. This can be mitigated by including resting times while milling to allow heating powders to cool down, and by choosing reactants with a low Gibbs free energy change during synthesis.

1.5 OBJECTIVES

The objective of this research is to provide a viable alternative to carbon-based anodes, ideally improving upon safety, tap density, and coulombic efficiency. Graphite is currently the preferred anode of choice due to its low cost and long cycle life, but it has safety issues related to formation of an SEI layer. This thesis work is focused on alloy anode materials, which are a well-studied alternative, but suffer from issues related to volume change during lithiation/delithiaton, leading to active material crumbling and particle agglomeration. Some methods which have previously been employed to mitigate these issues are reducing the particle size down to the nanoscale, and the use of an inactive buffer matrix material. These methods have been combined in a procedure utilizing high energy mechanical milling to perform mechanochemical synthesis of nanostructured Sn-based anodes with a TiC-C buffer matrix. Our goal is to utilize these strategies to synthesize an alloy anode with cycle life comparable to graphite, but with higher capacity and less safety issues.

To truly be competitive with graphite as an anode, an anode material must have a relatively low cost of production. This can be achieved by utilizing simple and scalable materials synthesis techniques. The cost of reactants is also a factor that was considered, as expensive or scarce materials would provide difficulties in scaling up material production, and would not be competitive with current battery materials on the market.

The synthesis utilized in this thesis involves simple, scalable methods: high energy mechanical milling and furnace heating. The materials required were all low cost: elemental Sn, Sb, Fe, Ti, and C. These methods were used to create nanostructured SnSb-

TiC-C and $FeSn_2$-TiC nanocomposites which demonstrate high capacity and tap density, as well as extended cycle life. The materials are characterized utilizing a variety of characterization techniques, including X-ray diffraction (XRD, energy dispersive spectroscopy (EDS), scanning electron microscopy(SEM), transmission electron microscopy (TEM), electrochemical charge-discharge measurements, and tap density measurements.

Chapter 2: Experimental Procedures

2.1 Materials Synthesis

SnSb-TiC-C nanocomposite alloy anodes were synthesized via high energy mechanical milling of the precursors that were prepared by heating in a furnace under argon atmosphere. $FeSn_2$-TiC nanocomposite alloy material was synthesized in a similar manner, utilizing high energy mechanical milling of heat treated precursors. The specific materials synthesis techniques will be elaborated upon further in the next chapter. The precursors for the materials prepared via HEMM were created by heating titanium with the other metals (Sn, Sb, and Fe depending on the material) at 800°C in a furnace under flowing argon for 6 hours. These mixtures were subjected to high energy mechanical milling under an argon atmosphere at room temperature for 48 hours at a speed of 500 rpm and a ball to powder ratio of 20:1

2.2 Materials Characterization Techniques

2.2.1 Scanning Electron Microscopy

Scanning electron microscopy (SEM) is a technique in which a high energy electron beam is rastered across the surface of a conductive sample, and the resulting signals are analyzed and converted into an image to identify surface morphology and microstructure of a sample. All SEM images shown in this thesis were taken by secondary electron detectors, which measure the electrons scattered by the impact of the

electron beam with the sample, drawing them into the detector with a low voltage bias. The scanning electron microscope used in this work was a JEOL JSM 5610 from Oxford Instruments.

2.2.2 Energy Dispersive Spectroscopy

Energy dispersive spectroscopy (EDS) is a technique often used in conjunction with a scanning electron microscope, which can be used to determine the elemental composition of a material. A high energy electron beam is again trained on the sample, but instead of secondary electrons, characteristic x-rays are measured by a photodetector. Characteristic x-rays are produced when the electron beam removes core electrons from the atoms within the sample. Electrons of higher energy levels will move into the vacated core electron state, and a photon will be given off which corresponds to the difference in energy between the two states. This X-ray photon will be of a distinct wavelength based on the difference between these two energy levels, which is different for every element and transition. The photodetector counts the number of x-rays of each wavelength, and these can be matched up using software to determine the relative amount of each element in the sample. EDS is not effective at measuring elements with low atomic number such as hydrogen or lithium, as these do not give off characteristic x-rays. The EDS detector used was attached to a JEOL JSM 5610 from Oxford Instruments.

2.2.3 TRANSMISSION ELECTRON MICROSCOPY

Transmission Electron Microscopy (TEM) utilizes a high energy electron beam passed through a thin sample to analyze materials. This was used to determine the particle size and crystallinity of the samples. The transmitted electron beam is deflected by atoms as it passes through a sample, and the deflected beams form an image based on this interaction. The TEM used in this project was a JEOL 2010 TEM operating at 300 kV.

2.2.4 X-RAY DIFFRACTION

X-ray diffraction (XRD) can be used to determine the crystal structure of a material, giving the phases present and lattice parameters. A beam of X-rays is diffracted off of a sample, which in our case consisted of powders resting on a glass slide. The angle between the x-ray beam, the sample, and the detector is gradually changed, and the diffracted x-rays are counted at each angle. The counts vs 2θ are plotted, which gives a distinct pattern for each crystal structure, obeying Bragg's law. This allows us to identify phases present in a material, and gives a sense of purity and crystallinity of phases. In this study, a Philips X-ray diffractometer was used with Cu Kα radiation.

2.2.5 CHARGE-DISCHARGE MEASUREMENTS

To analyze the electrochemical properties of the SnSb-TiC-C and FeSn2-TiC materials, electrodes were prepared by creating a slurry with 70 wt. % active material, 15 wt. % conductive carbon (Super P) and 15 wt. % polyvinylidine fluoride (PVDF)

dissolved in N-methyl pyrrolidone (NMP) as a binder. Electrodes were made by spreading this slurry on a Cu foil with a doctor blade, and drying for 24 hours at 120° C in a vacuum oven. The electrodes were assembled in CR2032 coin cells in an Ar-filled glovebox with the cast electrode as the working electrode, lithium foil as the counter electrode, Celgard polypropylene seperator, and 1 M $LiPF_6$ in ethylene carbonate (EC)/diethyl carbonate (DEC) (1 : 1 v/v) as the electrolyte. The discharge/charge cycling experiments were performed at a constant current density of 100 mA g-1 with an Arbin battery cycler, over a voltage range of 0-2.0V vs. Li/Li^+.

2.2.6 TAP DENSITY MEASUREMENTS

Tap density is a measurement of the density of compact powders, usually measured in g cm^{-3}. A tap density test is performed by weighing out a powder and transferring it to a graduated cylinder. The graduated cylinder is then subjected to tapping on a sturdy surface, to compact the powder. 100 taps were typically used for our research. Once the powder has been compacted, the volume is measured in the graduated cylinder, and the tap density is calculated from the weight and volume measured. A Quantachrome AT-4 Autotap density measurer was used for all values given in this report.

Chapter 3: SnSb-TiC-C and $FeSn_2$-TiC Nanocomposite Anodes

3.1 Introduction

The two electrode powders primarily investigated during this research were a nanocomposite composed of SnSb, TiC, and C, and another nanocomposite composed of $FeSn_2$ and TiC. SnSb is composed of two electrochemically active elements, which are known for their high theoretical capacities when reacting with lithium: Sn ($Li_{4.4}Sn$: 990 mAh g^{-1}) and Sb (Li_3Sb: 660 mAh g^{-1}). Since Sn and Sb will both undergo volume expansion during lithiation/delithiation, the active SnSb does not have the same inactive buffer matrix that would be present in an active-inactive composite such as $FeSn_2$ or Cu_2Sb. However, the Sn and Sb being constrained in the nanoscale can prevent particle agglomeration of Sn and Sb upon cycling. In addition, the particles can rely on the TiC and C matrix to prevent agglomeration of particles, and to act as a buffer during volume expansion caused by cycling. SnSb-TiC-C was synthesized by a high energy mechanical milling (HEMM) method. For the HEMM method, TiSn and TiSb precursors were prepared by heating in a furnace under flowing argon, then mixed with acetylene black carbon and subjected to high energy mechanical milling. The ratios of active material : TiC : C were modified, and the best performance was found at a weight percent of 40% SnSb : 40% TiC : 20% C.

$FeSn_2$ is an active-inactive intermetallic alloy material, in which the Fe acts as a buffer matrix while the Sn reacts with lithium. The reported reaction mechanism for $FeSn_2$ is a conversion reaction, where the inactive component is extruded and forms a reinforcing matrix, and the active material is allowed to be lithiated. The TiC in the nanocomposite serves as a buffer matrix, and also prevents agglomeration of particles, keeping the particle size on the nanoscale to mitigate volume expansion issues. The $FeSn_2$-TiC sample was synthesized through a high energy mechanical milling (HEMM) method. Ti/Sn and Ti/Fe precursors were prepared by heating in a furnace under flowing argon, then mixed with acetylene black carbon and subjected to high energy mechanical milling, with stoichiometric carbon added so that it would be incorporated into the TiC matrix, with no excess carbon remaining. The ratios of active material : TiC were modified, and the best performance was found at a weight percent ratio of 50% TiC : 50% $FeSn_2$.

A sample with Fe, Sn, and C was also prepared through HEMM for comparison purposes, though the precursors were not heated beforehand. For this sample, the weight percents were constructed to make 50% $FeSn_2$ and 50% C. Samples were also prepared of Sn-TiC and Sb-C for comparative purposes.

The SnSb particles suspended in the TiC-C matrix and the SnSb-TiC-C nanocomposite were characterized by X-ray diffraction (XRD), scanning electron microscopy (SEM), energy dispersive spectroscopy (EDS), transmission electron microscopy (TEM), and electrochemical charge-discharge measurements.

3.2 EXPERIMENTAL

The SnSb-TiC-C composite was prepared as follows. For the HEMM method, TiSn and TiSb precursors were prepared in a furnace under flowing argon by heating elemental Sn (99.8% < 45 μm, Aldrich), Sb (99.9 %, Aldrich), and Ti (99.99%, ~ 325 mesh, Alfa Aesar). The precursors were prepared with enough Ti, Sn, and Sb so that the final product would have a weight percent of 40% SnSb : 40%TiC:20%C with the Ti distributed evenly between the two precursors. The Ti-Sb precursor contained Ti : Sb = 2.7 : 1 and the Ti-Sn precursor contained Ti : Sn = 2.7 : 1. The precursors were then mixed with acetylene black and subjected to high energy mechanical milling under an argon atmosphere at room temperature for 48 hours at a speed of 500 rpm and a ball to powder ratio of 20:1

The $FeSn_2$-TiC composite was synthesized by heating a mixture of Sn and Ti as well as a mixture of Sn and Fe (99.9%, <10 μm, Alfa Aesar) in a flowing argon atmosphere at 800°C for 6 hours. The Ti-Sb precursor contained an atomic ratio of Fe : Ti = 4 : 3, and the Ti-Sn precursor contained Ti :Sn = 2 : 1. The Fe-Ti and Sn-Ti mixtures were then mixed with a stoichiometric amount of carbon (Alfa Aesar, acetylene black, 99.99%, -200 mesh) to create a composite material with 50% TiC and 50% $FeSn_2$ by weight. This mixture was subjected to high-energy mechanical milling (HEMM) under an argon atmosphere at room temperature for 48 hours at a speed of 500 rpm and a ball to powder ratio of 20 : 1. Sn-TiC and Sb-C electrode powders were also synthesized via HEMM for comparative purposes, under the same parameters utilizing unheated powders of Sn, Sb,

and C. The pure graphite used for electrochemical testing was Conoco Philips CPreme G8.

The synthesized composite powder morphology was analyzed utilizing a JEOL JSM-5610 scanning electron microscope (SEM) and a JEOL 2010F high-resolution transmission electron microscope (HRTEM) operating at 300 kV. The electrode powder was characterized by X-ray diffraction (XRD) using a Philips X-ray Diffractometer with Cu-Kα radiation. To analyze the electrochemical properties of the SnSb-TiC-C and $FeSn_2$-TiC materials, electrodes were prepared by creating a slurry with 70 wt. % active material, 15 wt. % conductive carbon (Super P) and 15 wt. % polyvinylidine fluoride (PVDF) dissolved in N-methyl pyrrolidone (NMP) as a binder. Electrodes were made by applying this slurry onto a Cu foil with a doctor blade and drying for 24 hours at 120° C in a vacuum oven. The electrodes were assembled in CR2032 coin cells in an Ar-filled glovebox with the cast electrode as the working electrode, lithium foil as the counter electrode, a Celgard polypropylene separator, and 1 M$LiPF_6$ in ethylene carbonate (EC)/diethyl carbonate (DEC) (1 : 1 v/v) as the electrolyte. The discharge/charge cycling experiments were performed at a constant current density of 100 mA g^{-1} with an Arbin battery cycler, over a voltage range of 0 - 2.0V vs. Li / Li^+. The TEM samples were prepared by dispersing the powder in ethanol via sonication, then depositing the solution on a copper grid and allowing the ethanol to air-dry. Cycle testing was performed with lithium metal as the reference electrode at a current density of 100 mA/g active material.

3.3 STRUCTURAL AND COMPOSITIONAL CHARACTERIZATION

Figures 3.1 shows the XRD patterns of the SnSb-TiC-C sample. The SnSb-TiC-C sample is shown to contain SnSb (stitstaite phase, space group: $Fm\bar{3}m$) with lattice constants of a = 5.88 Å, b = 5.88 Å, c = 5.88 Å (JCPDS File: 00-026-0115), as well as crystalline TiC (khamrabaevite phase, space group: $Fm\bar{3}m$), with lattice constants of a = 4.33 Å, b = 4.33 Å, c = 4.33 Å (JCPDS File: 00-031-1400. No peaks for carbon were seen, suggesting that it is amorphous within the electrode powder or mostly incorporated into the titanium carbide phase.

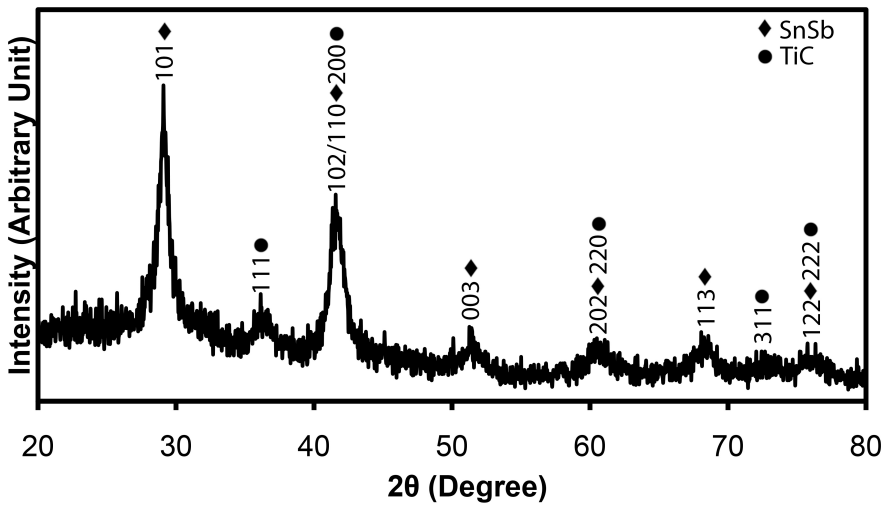

Figure 3.1: XRD pattern of the SnSb-TiC-C nanocomposite synthesized via HEMM.

The $FeSn_2$-TiC-C sample consists of $FeSn_2$ particles (space group: I4/mcm) with lattice constants of a = 6.545Å, b = 6.545Å, c = 5.326Å (JCPDS File: 01-071-7852). The $FeSn_2$-TiC sample demonstrates good purity with few residual precursor peaks. Both

patterns show peaks corresponding to crystalline TiC (khamrabaevite phase, space group: $Fm\bar{3}m$), with lattice constants of a = 4.33 Å, b = 4.33 Å, c = 4.33 Å (JCPDS File: 00-031-1400. No peaks for carbon were seen in this sample, suggesting that it is amorphous within the electrode powder or mostly incorporated into the titanium carbide phase.

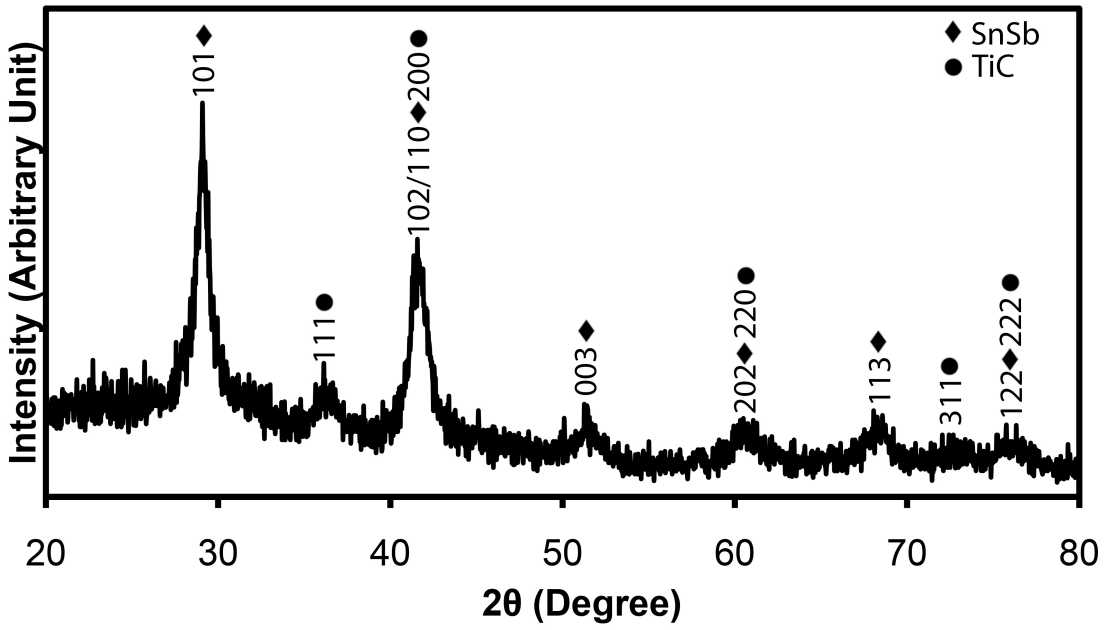

Figure 3.2: XRD pattern of the $FeSn_2$-TiC-C nanocomposite synthesized via HEMM.

SEM micrographs were taken of the SnSb-TiC-C and $FeSn_2$-TiC powders, shown in Figure 3.3(a-b). The powders appear structurally similar and are composed of roughly spherical particles, with sizes ranging from 10 microns to nanometer-scale particles. The two powders appear to have similar topography to each other at 1000x

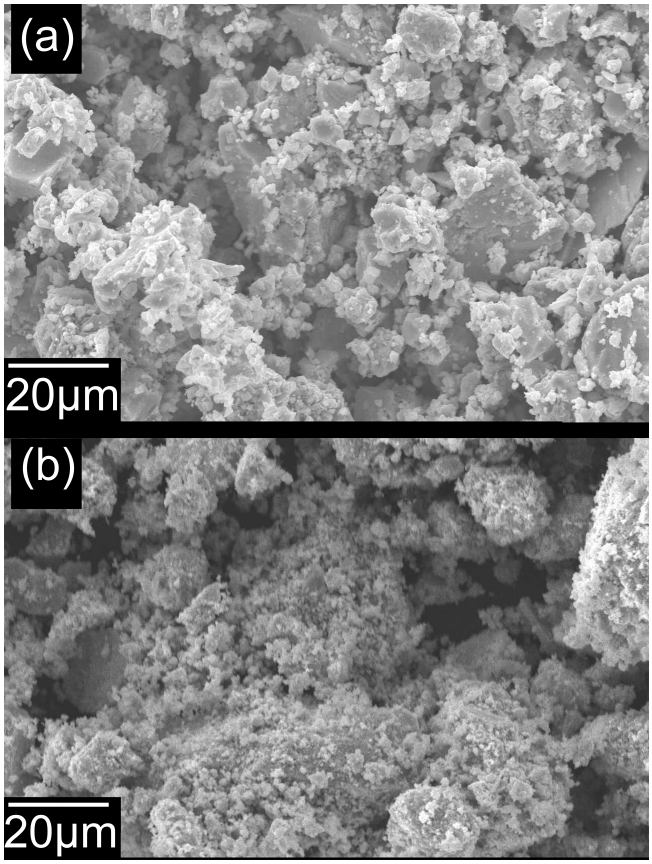

Figure 3.3: SEM images of (a) SnSb-TiC-C electrode powder and (b) $FeSn_2$-TiC electrode powder under 1000x magnification.

Figure 3.4 shows the EDS elemental maps from Sn, Sb, and Ti of the SnSb-TiC-C sample. To obtain these elemental maps, the electron beam is rastered across the sample surface, and the characteristic x-rays are measured by the detector at each point, with the points where radiation is detected showing up as white on the image. The Sn and Sb image show peaks from the Lα transition, and the Ti image shows peaks obtained from the Kα transition. The EDS data confirm that the elements are evenly distributed throughout the bulk of the sample, and there are no large clusters of carbon or TiC. A

similar distribution was seen for the $FeSn_2$-TiC sample, with Fe, Sn, Ti, and C evenly distributed through the microstructure.

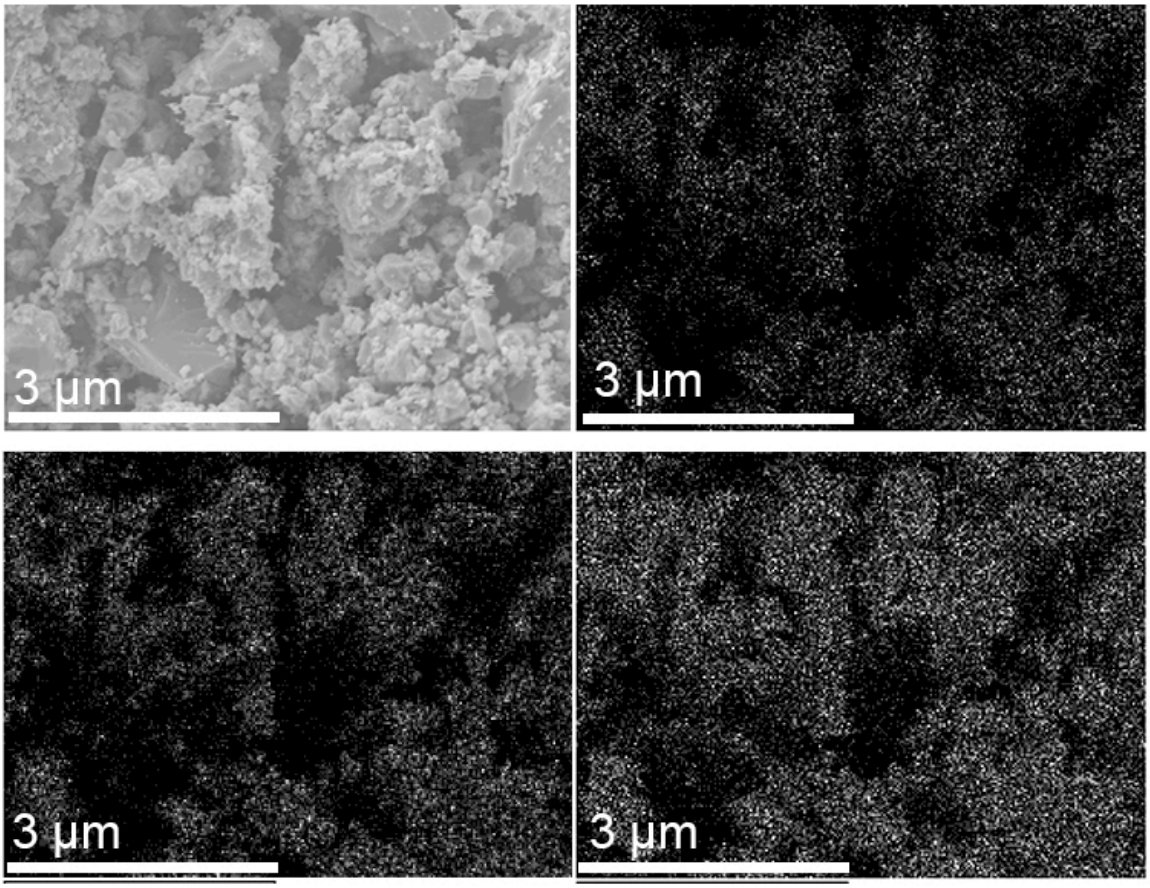

Figure 3.4: EDS spectra of SnSb-TiC-C powder: (a) secondary electron image, (b) Sb Lα1 signals, (c) Ti Kα1 signals, and (d) Sn Lα1 signals.

Figure 3.5 shows a TEM image of an agglomerate composed of crystallites of $FeSn_2$ and TiC from the $FeSn_2$-TiC sample with a diameter of ~ 90 nm. The particle appears to be coated with a layer of TiC, though lattice fringes could not be seen in the small

particle. A diffraction pattern from the bulk powder is shown in the inset, confirming the presence and crystalline nature of $FeSn_2$ and TiC.

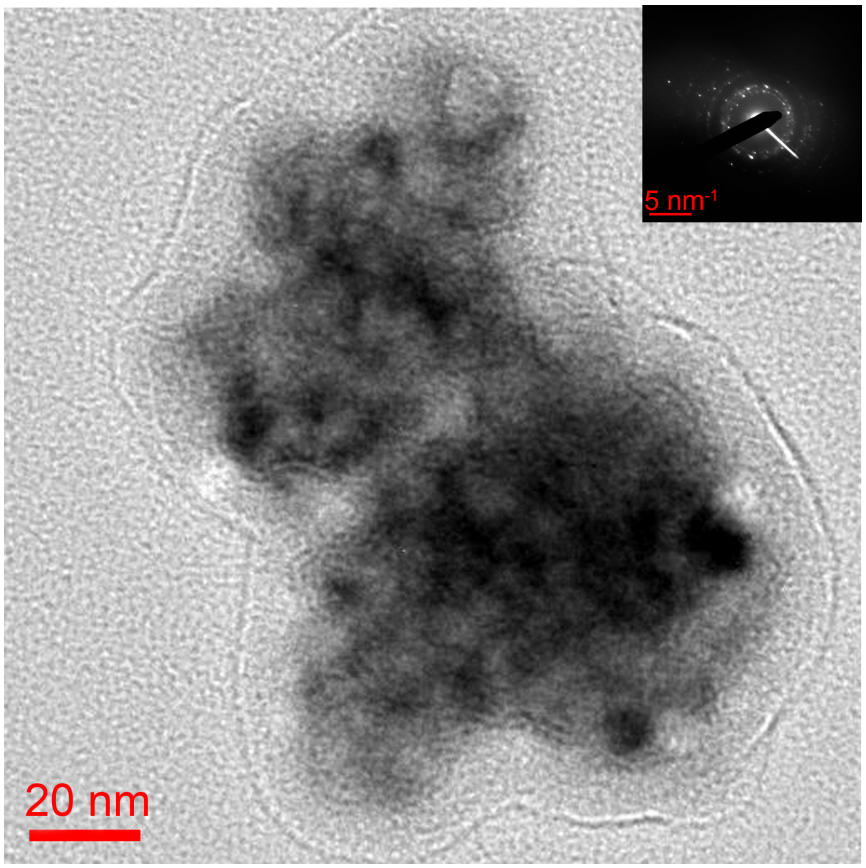

Figure 3.5: TEM image of as-synthesized $FeSn_2$-TiC nanoparticles, showing crystalline $FeSn_2$ in a TiC matrix.

Figure 3.6 shows a TEM image of an agglomerate composed of crystallites of SnSb, TiC, and C with a diameter of ~ 250 nm. A bulk powder diffraction pattern is shown in the corner of this image, confirming the presence of crystalline SnSb and TiC. The

inactive buffer matrix formed around individual particles is ideal to prevent agglomeration of particles and volume expansion issues.

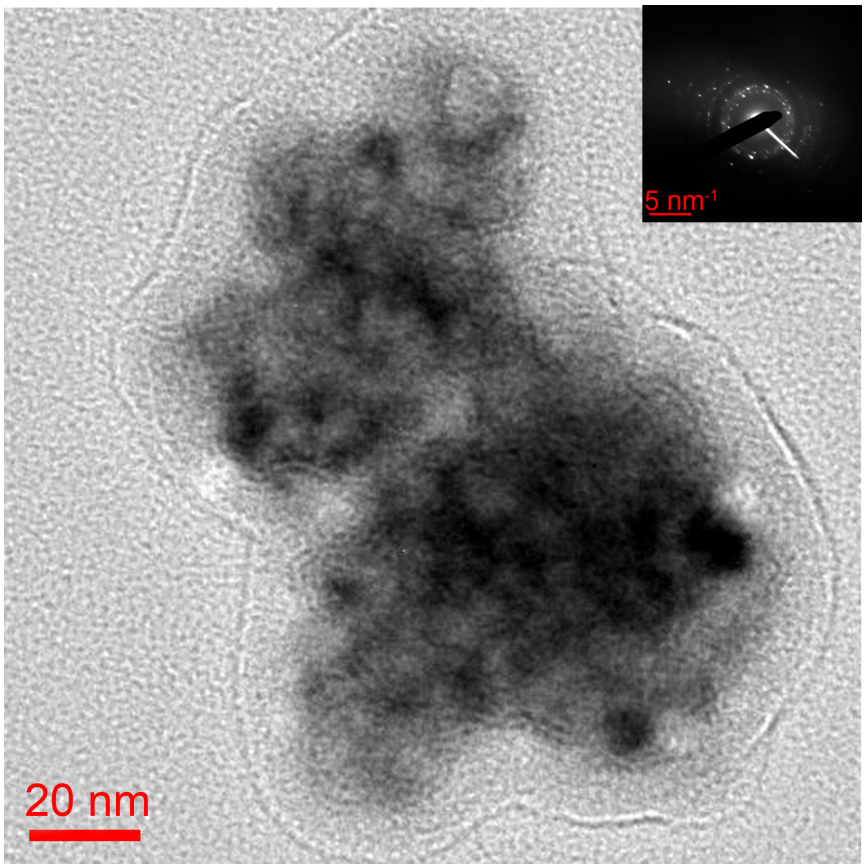

Figure 3.6: TEM image of as-synthesized SnSb nanoparticles, showing crystalline SnSb in a TiC-C matrix.

Assuming that the materials synthesized are pure as confirmed by TEM and XRD, the SnSb-TiC-C sample should be composed of 40 wt. % SnSb, 40 wt. % TiC, and 20 wt. % C. Taking SnSb and C as the active materials and utilizing theoretical specific capacities of 824 mAh g^{-1} for SnSb and ~ 400 mAh g^{-1} as seen with half-cell testing of

acetylene black carbon, the SnSb-TiC-C has a theoretical specific capacity of 404 mAh g^{-1}. Similarly, assuming a specific capacity of ~ 100 mAh g^{-1} as seen with half-cell testing of TiC synthesized via HEMM, the $FeSn_2$-TiC electrode powder should have a theoretical specific capacity of ~ 450 mAh g^{-1}.

3.4 Electrochemical Characterization

Figures 3.7a and 3.7b shows the volumetric and gravimetric capacities with cycle number for the SnSb-TiC-C nanocomposite sample compared to that of graphite powder. The SnSb-TiC-C exhibit excellent capacity and cycle life, with an initial discharge capacity of 769 mAh g^{-1}(1385 mAh cm^{-3}) and an initial charge capacity of 517 mAh g^{-1} (930 mAh cm^{-3}), yielding an initial coulombic efficiency of 85%. There appeared to be continued capacity fade on subsequent cycles, but the sample retained a specific capacity of 392 $mAhg^{-1}$ (705 mAh cm^{-3}) after 100 cycles. The sample demonstrate better cycle life and coulombic efficiency compared to that previously published for pure SnSb anodes and higher volumetric and gravimetric capacities than graphite, while still retaining a high tap density of 1.8 $mAhg^{-1}$.[7,9]

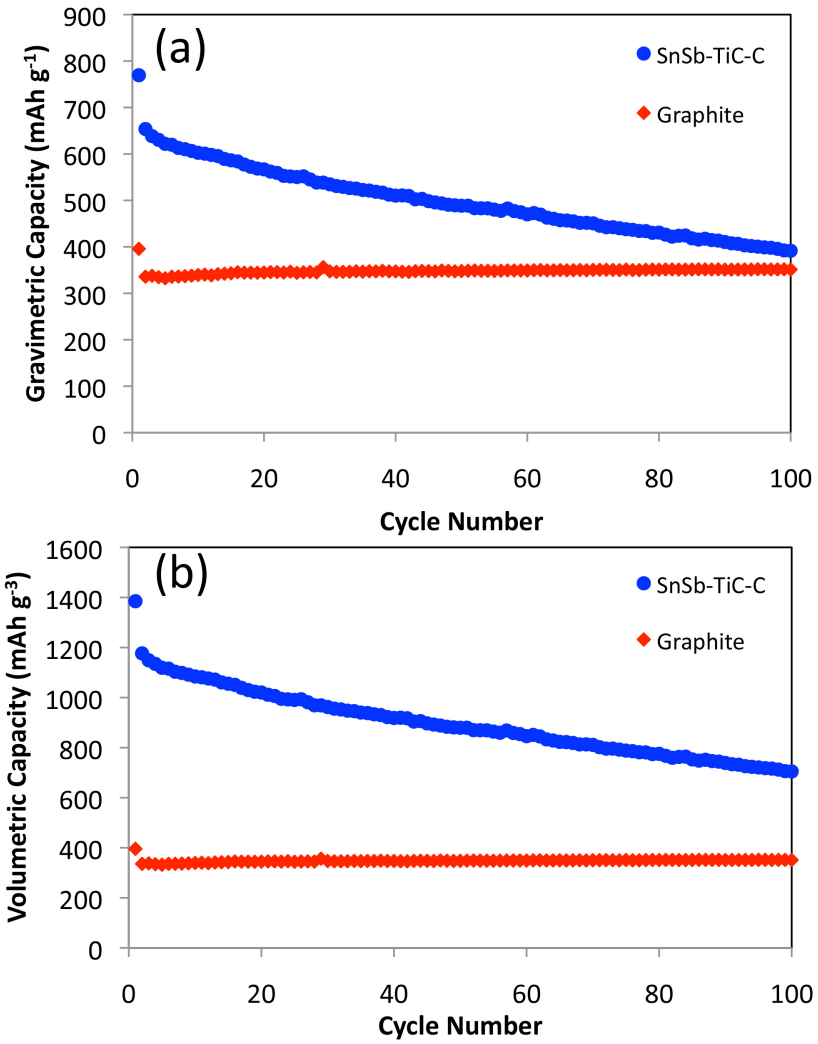

Figure 3.7: (a) Long-term cycling performance of SnSb-TiC-C at 0 – 2.0 V vs. Li/Li+ at 100 mA g^{-1} compared to the performance of graphite under the same conditions and (b) long-term cycling performance (volumetric capacity) of SnSb-TiC-C at 0 – 2.0 V vs. Li/Li+ at 100 mA g-1 compared to the performance of graphite under the same conditions.

Figure 3.8 shows a comparison of the SnSb-TiC-C samples with an Sn-TiC sample (35 wt. % Sn, 65 wt. % TiC) and an Sb-C sample (80 wt. % Sb, 20 wt.% C). The initial discharge capacity of SnSb-TiC-C (769 mAh g^{-1}) is significantly greater than that of the Sn-TiC or Sb-C samples which showed, respectively, initial gravimetric capacities of 693 and 431 mAh g^{-1}. This is most likely due to the greater proportion of Sn, which has a theoretical reversible capacity of 990 mAh g^{-1}. SnSb-TiC-C also exhibits significantly less capacity fade over time than the Sn-TiC or Sb-C samples, as well as pure SnSb reported in the literature.[26] This is due to the TiC-C matrix forming a protective buffer around the SnSb active material nanoparticles.

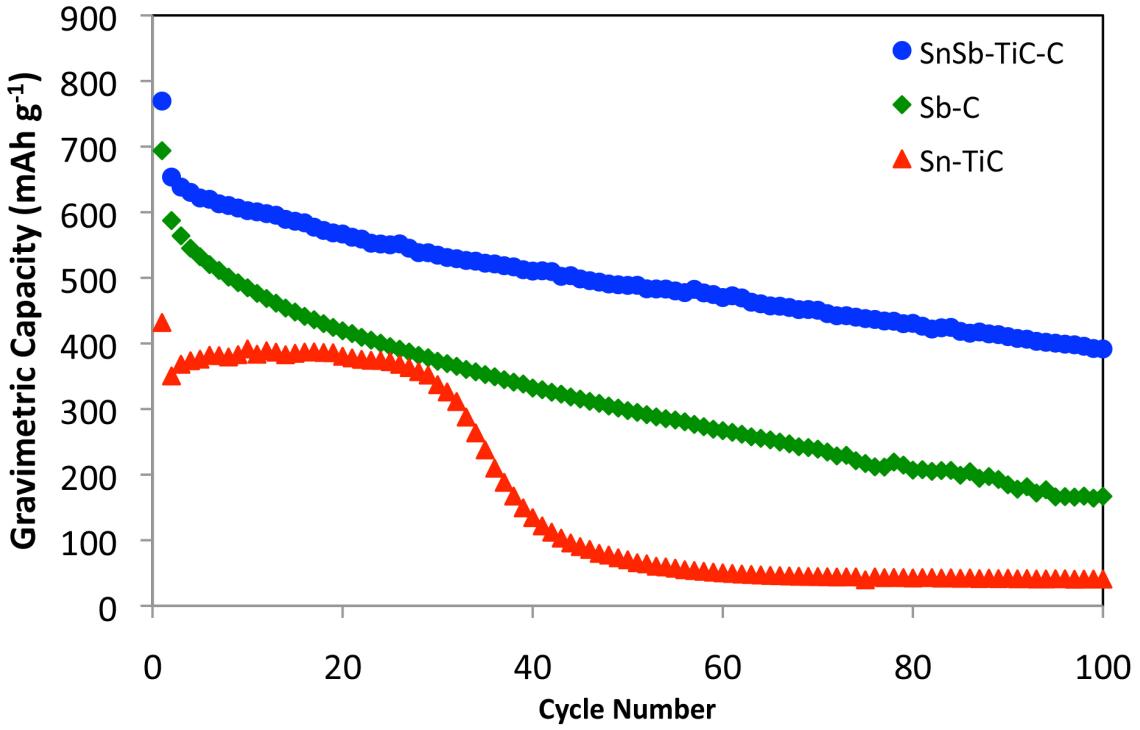

Figure 3.8: Long-term cycling performance (gravimetric capacity) of SnSb-TiC-C at 0 – 2.0 V vs. Li/Li+ at 100 mA g^{-1} compared to the performance of Sn-TiC and Sb-C under the same conditions.

The carbon-free Sn-TiC sample prepared via HEMM began failing after only 30 cycles, likely because the pure TiC matrix could not accommodate the volume expansion without excess carbon. The Sb-C sample showed a significantly faster decline in capacity than the SnSb-TiC-C material, the difference in gravimetric capacity between the two materials

was 75 mAh g^{-1} after the first cycle, but 217 mAh g^{-1} after 100 cycles. This excellent extended cycle life is an improvement upon bulk SnSb anodes, and is comparable to the extended cycling performance of SnSb/C anodes.[23] In addition, the high tap density (1.8 g cm^{-3}) of the SnSb-TiC-C nanocomposite gives it superior volumetric capacity compared to the SnSb/C anodes due to the higher density of TiC, leading to higher volumetric capacity.

The voltage profiles for the first five cycles of this sample are seen in Figure 3.9. The most significant irreversible capacity can be seen in the first cycle, with most occurring below 0.4 V, where SEI layer formation typically occurs. The low voltage plateau decreases in the 2^{nd}-5^{th} cycles, as the SEI layer has already been formed, with the bulk of the capacity coming from reversible lithiation and delithiation of the Sb and Sn. Some irreversibility can also be attributed to the reduction of electrolyte on the surface of the sample during cycling.

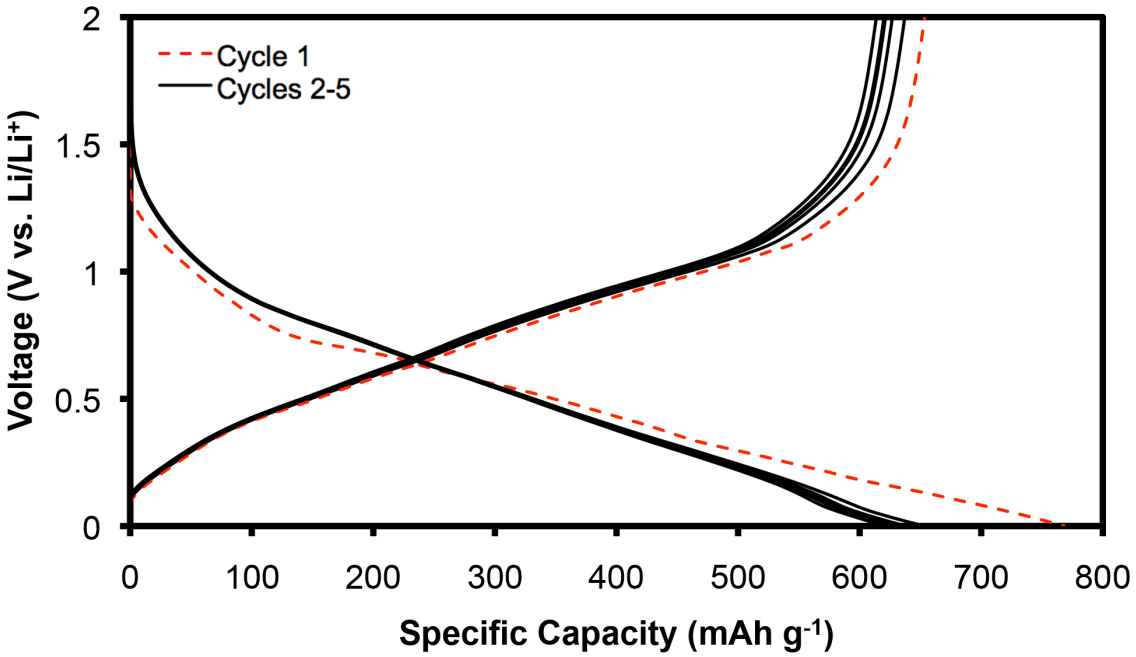

Figure 3.9: Voltage vs. capacity plot of SnSb-TiC-C at 0 – 2.0 V.

The differential capacity plot of the SnSb-TiC-C system is given in Figure 3.10a - 3.10c. Reaction peaks for the discharge curves after the first cycle are seen at ~ 0.2 – 0.4 V and ~ 0.7 V, which can be attributed to lithiation of Sn.[23] A peak is also seen at ~ 0.8 V vs Li/Li$^+$, which corresponds to lithiation of Sb.[31,34] Figures 3.10a and 3.10b show the differential capacity plots for Sn-TiC and Sb-C powders prepared through HEMM, which demonstrate lithiation peaks at similar voltages. Figure 3.10c shows the differential capacity plot for SnSb-TiC-C, with lithiation peaks at similar locations. Charge peaks for Sn-TiC and SnSb-TiC-C occur at ~ 0.4 and 0.6, which can be attributed to the reaction of Sn. Delithiation peaks appear in the Sb-C and SnSb-TiC-C powders at 1 V v vs. Li / Li$^+$,

which can be attributed to the reaction of Sb. These peak locations are also seen in Figure 3.10c. This serves to confirm that the reaction proceeds in two steps as described in

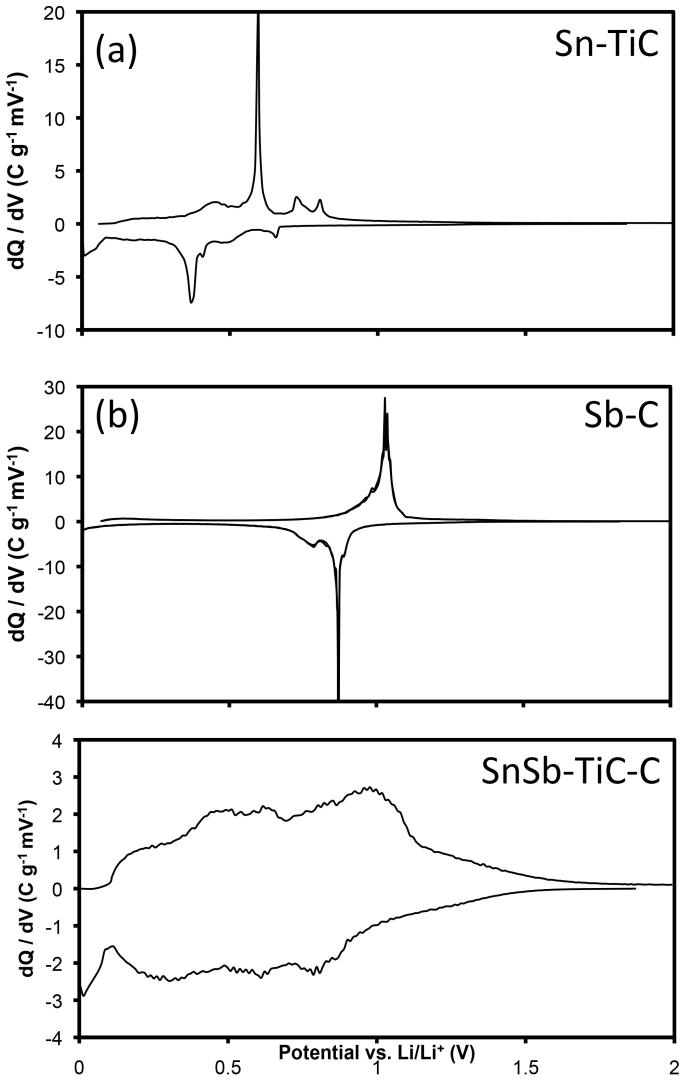

Figure 3.10: Differential capacity plots of the 3rd cycle of (a) SnSb-TiC-C, (b) Sb-C, and (c) Sn-TiC.

equations 1 and 2, with the Sb first reacting at a higher potential, followed by the Sn. The broader peaks for the SnSb-TiC-C sample compared to that in the Sn-TiC and Sb-C samples suggest a smaller crystalline particle size in the SnSb nanocomposite, which can also contribute to improved cycle life.

Gravimetric and volumetric capacities for the $FeSn_2$-TiC electrode powder are shown in Figure 3.11. The $FeSn_2$-TiC sample exhibit an initial discharge capacity of 511 $mAhg^{-1}$ and an initial charge capacity of 381 mAh g^{-1}, yielding an initial coulombic efficiency of 75% and an irreversible capacity of 113 mAh g^{-1}. The sample shows a consistent

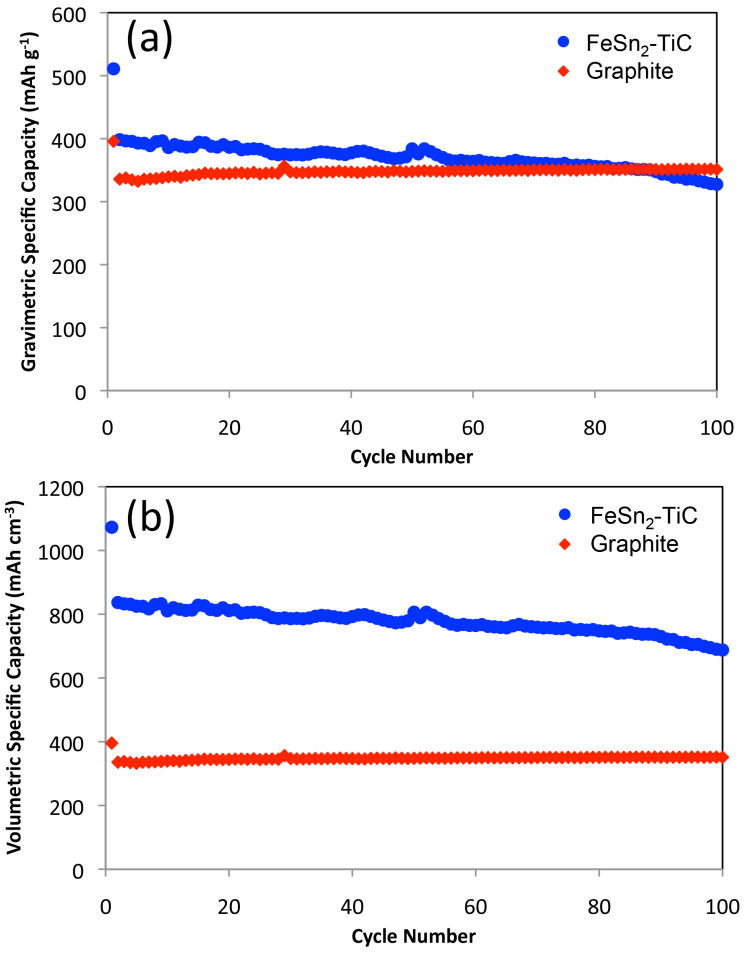

Figure 3.11: (a) Long-term cycling performance (gravimetric capacity) of $FeSn_2$-TiC at 0 – 2.0 V vs. Li/Li^+ at 100 mA g^{-1} compared to the performance of graphite under the same conditions and (b) long-term cycling performance (volumetric capacity) of $FeSn_2$-TiC at 0 – 2.0 V vs. Li/Li^+ at 100 mA g^{-1} compared to the performance of graphite under the same conditions.

coulombic efficiency of over 98% after the fifth cycle. The tap density measured was 2.1 g cm^{-3}, giving a significantly higher volumetric capacity than graphite, and a comparable gravimetric capacity to graphite after extended cycling. Figure 3.12 compares the capacity of $FeSn_2$-TiC to Sn-TiC. The $FeSn_2$-TiC nanocomposite shows similar capacity for the first few cycles, but the Sn-TiC sample begins to fail after 30 cycles while the $FeSn_2$-TiC sample remains stable for 100 cycles. It is likely that the extended cycle life is due to the alloying of tin with the inactive Fe which is extruded during lithiation as

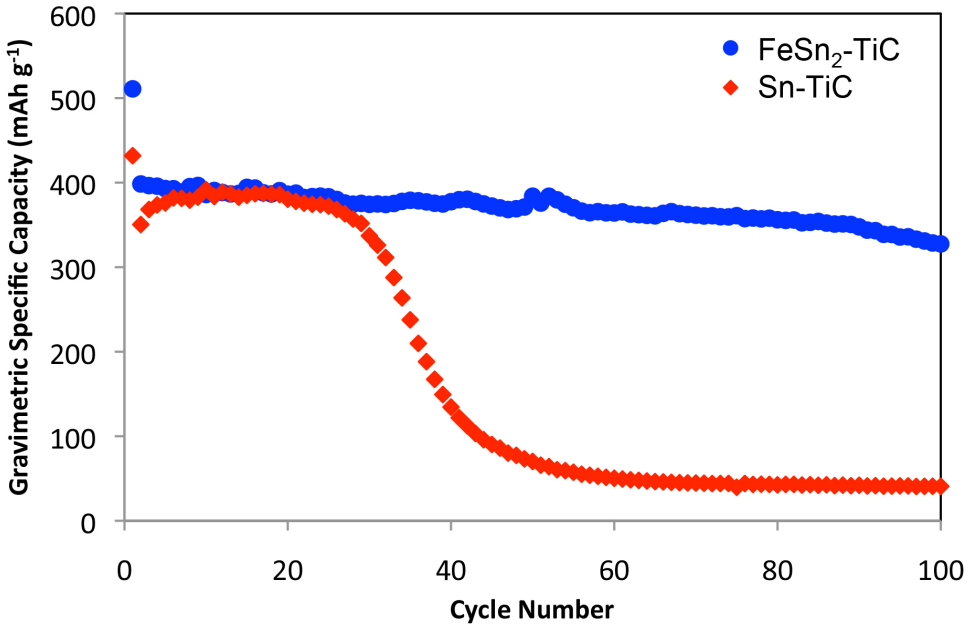

Figure 3.12: Long-term cycling performance (gravimetric capacity) of $FeSn_2$-TiC at 0 – 2.0 V vs. Li/Li^+ at 100 mA g^{-1} compared to the performance of Sn-TiC under the same conditions.

described in equations 3 and 4, forming an inactive buffer matrix that inhibits crumbling and delamination of the active material. The TiC serves to provide additional resistance to particle expansion and agglomeration of the Sn particles. A Sn-TiC-C nanocomposite material synthesized via HEMM was reported by our group before with similar capacity[25], but the electrode powders reported required 20 wt. % excess carbon. Carbon-free electrode powders such as the $FeSn_2$-TiC nanocomposite are ideal because they can prevent issues associated with carbon anodes, such as low tap density and coulombic efficiency, and can operate at higher reaction potentials. A Fe-Sn/C nanocomposite anode synthesized via HEMM was reported by Yoon *et al*[35] with 17 wt. % excess C. The Fe-Sn/C anode exhibited a specific capacity of 380 mAh g^{-1} after 100 cycles, but had an irreversible capacity loss of ~ 300 mAh g^{-1} after the first two cycles. The $FeSn_2$-TiC had an irreversible capacity loss of 115 mAh g^{-1} after two cycles, demonstrating the superior Coulombic efficiency that can be obtained by utilizing TiC as an alternative buffer matrix material to carbon.

The voltage profiles for the first five cycles of the $FeSn_2$-TiC sample are seen in Fig. 3.13. The irreversible capacity can be seen in the first cycle, with the most significant irreversibility occurring below 0.2 V vs Li/Li^+, which can be attributed to SEI layer formation and surface electrolyte reduction. The low voltage plateau is considerably less shallow in the 2^{nd}-5^{th} cycles, leveling out at ~ 0.4 V vs. Li/Li^+. The 2^{nd}-5^{th} cycles show the alloying and dealloying of Sn occurring mostly over a potential range of 0.2 – 1.5 V, which is consistent with the profiles seen in the literature for Sn-TiC-C.[15]

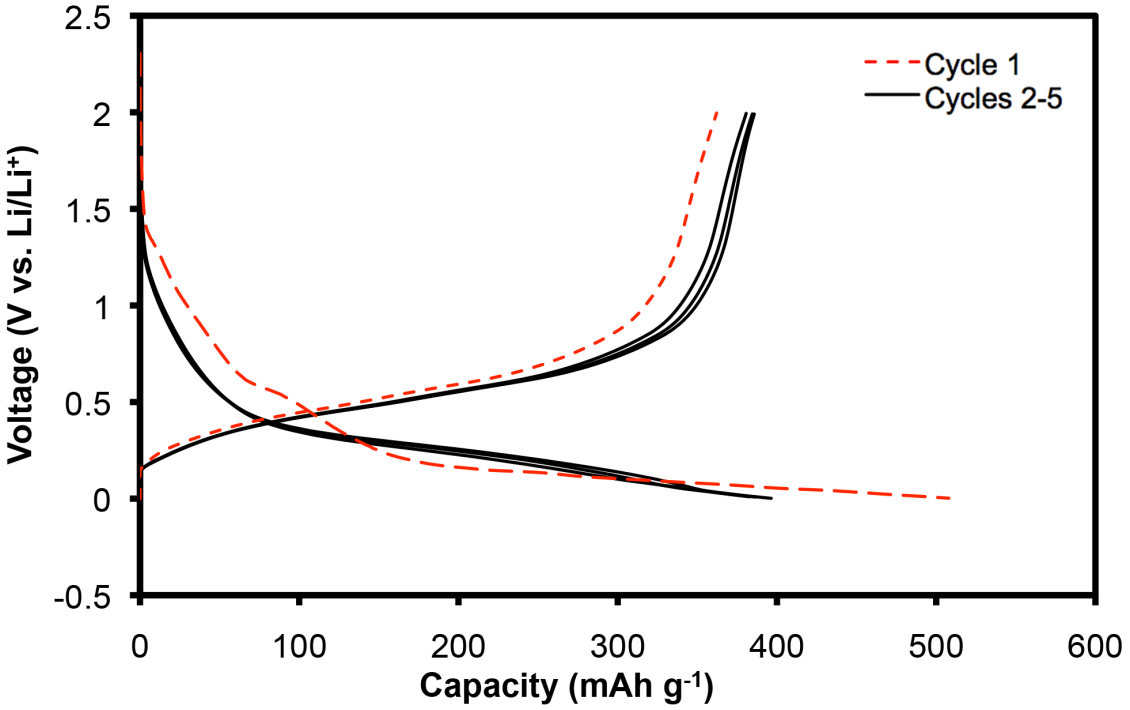

Figure 3.13: Voltage vs. capacity plots of FeSn2-TiC at 0 – 2.0 V.

Figure 3.14a illustrates the differential capacity plot for the $FeSn_2$-TiC-C nanocomposite, contrasted with a differential capacity plot for Sn-TiC in Figure 3.14b. The reaction peaks in the discharge curve of Sn-TiC occur at voltages corresponding with Sn lithiation, at ~ 0.2 – 0.4V vs. Li / Li^+. The reaction peaks at the charge curve occur at ~ 0.4 – 0.65 V. vs Li / Li^+, which again correspond with the alloying of Sn. The peaks observed for $FeSn_2$-TiC seem to match the voltages observed for Sn-TiC, suggesting that it corresponds to the lithiation and delithiation of Sn that is responsible for the reversible capacity. These peak locations are in agreement with the differential capacity plots for $FeSn_2$-based materials seen in the literature.[22,27,34]

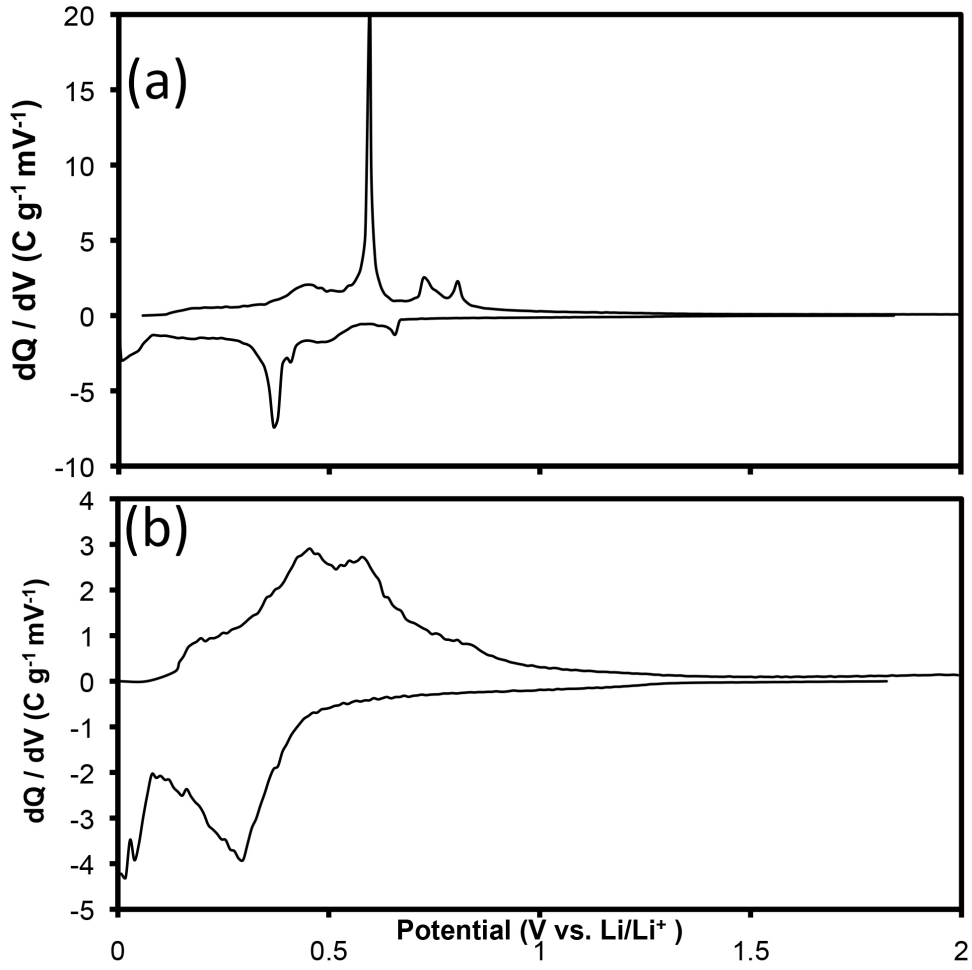

Figure 3.14: Differential capacity plots of the 3rd cycle of (a) $FeSn_2$-TiC and (b) Sn-TiC.

3.5 CONCLUSIONS

SnSb-TiC-C and $FeSn_2$-TiC nanocomposite anodes have been synthesized via a HEMM method and characterized by XRD, SEM, and TEM. This characterization revealed that the SnSb-TiC-C sample is composed of nanoscale particles of SnSb surrounded by a reinforcing matrix of TiC and C, and the $FeSn_2$-TiC sample is composed

of nanoscale SnSb surrounded by a reinforcing TiC matrix. The SnSb-TiC-C nanocomposite exhibits significantly better cyclability than pure nanoscale SnSb, retaining a capacity of ~ 400 mAh g^{-1} after 100 cycles, an initial Coulombic efficiency of 85%, and a tap density of 1.8 mAh g^{-1}. The $FeSn_2$-TiC nanocomposite demonstrates excellent cyclability up to 100 cycles, with an initial Coulombic efficiency of 75%. The $FeSn_2$-TiC sample retains a gravimetric discharge capacity of over 325 mAh cm^{-3} for 100 cycles with a tap density of 2.1 $mAhg^{-1}$. Due to these high capacities, good cycle life, and high tap density, the SnSb-TiC-C and $FeSn_2$-TiC represent viable alternatives to graphite anode for lithium-ion batteries.

References

1. Tarascon, J.-M. & Armand, M. Issues and challenges facing rechargeable batteries. *Nature* **2001**, 414, 359–367
2. Manthiram, A. Materials Challenges and Opportunities of Lithium ion Batteries. *J. Phys. Chem. Lett.* **2011,** *2,* 176-184.
3. Zhang, W.-J. A review of the electrochemical performance of alloy anodes for lithium-ion batteries. *J. Power Sources.* **2011,** *196,* 13-24.
4. Goodenough, J. B.; Kim, Y. Challenges of Rechargeable Lithium Batteries. *Chem. Mater.* **2010,** *22,* 587–603.
5. Z. X. Shu, R. S. McMillan, and J. J. Murray. Electrochemical Intercalation of Lithium into Graphite. *J. Electrochem. Soc.* **1993***, 140,* 922-927.
6. G. Derrien, J. Hassoun, S. Panero and B. Scrosati. A Nanostructured Sn–C Composite Lithium Battery Electrode with Unique Stability and High Electrochemical Performance. *Adv. Mater.,* **2007,** *19,* 2336.
7. M. Wachtler, J.O. Besenhard, M. Winter. Tin and tin-based intermetallics as new anode materials for lithium-ion cells. *J. Power Sources,* **2001***, 94,* 189
8. R. Retoux, T. Brousse and D.M. Schleich. High-Resolution Electron Microscopy Investigation of Capacity Fade in SnO2 Electrodes for Lithium-Ion Batteries *J. Electrochem. Soc.,* **1999,** *146,* 2472.
9. M. Winter and J. O. Besenhard. Electrochemical lithiation of tin and tin-based intermetallics and composites. *Electrochim. Acta,* **1999,** *45,* 31.

10. U. Kasavajjula, C. Wang, A.J. Appleby. Nano-and bulk-silicon-based insertion anodes for lithium-ion secondary cells. *J. Power Sources,* **2007,** *163,* 1003.

11. D. Fauteux, R. Koksbang. Rechargeable lithium battery anodes: alternatives to metallic lithium. *J. Appl. Chem.* **1993,** *23,* 1.

12. Ji, L.; Lin, Z.; Alcoutlabi, M.; Zhang, X. Recent developments in nanostructured anode materials for rechargeable lithium-ion batteries. *Energy Environ. Sci***. 2011,** *4,* 2682-2699.

13. Naichao Li, Charles R. Martin, and Bruno Scrosati. A High-Rate, High-Capacity Nanostructured Tin Oxide Electrode. *Electrochem. Solid-State Lett.* **2000,** *3,* 316-318

14. D. Applestone and A. Manthiram, Cu6Sn5-TiC-C Nanocomposite Alloy Anodes with High Volumetric Capacity for Lithium-Ion Batteries, *RSC Advances.* **2012,** *2,* 5411-5417.

15. S. Yoon and A. Manthiram, Nanoengineered Sn-TiC-C Anode for Lithium-Ion Batteries, *Journal of Materials Chemistry.* **2010,** *20*, 236-239.

16. E. Allcorn and A. Manthiram, NiSb-Al2O3-C Nanocomposite Anodes with Long Cycle Life for Li-ion Batteries, *Journal of Physical Chemistry C.* **2014,** *118,* 811-822.

17. E. Allcorn and A. Manthiram, FeSb2-Al2O3 Nanocomposite Anodes for Lithium-ion Batteries, ACS Applied Materials & Interfaces.

18. D. Applestone, S. Yoon, and A. Manthiram, “Cu2Sb-Al2O3-C Nanocomposite Alloy Anodes with Exceptional Cycle Life for Lithium-Ion Batteries,” *Journal of Materials Chemistry.* **2012,** *22,* 3242-3248.

19. Ji, L.; Lin, Z.; Alcoutlabi, M.; Zhang, X. Recent Developments in Nanostructured Anode Materials for Rechargeable Lithium-Ion Batteries. *Energy Environ. Sci.* **2011***, 4*, 2682-2699.

20. Park, C.-M.; Kim, J.-H.; Kim, H.; Sohn, H.-J. Li-Alloy Based Anode Materials for Li Secondary Batteries. *Chem. Soc. Rev.* **2010,** *39,* 3115-3141.

21. Courtney, Ian A., and J. R. Dahn. "Electrochemical and in situ X-ray diffraction studies of the reaction of lithium with tin oxide composites." *Journal of the Electrochemical Society.* **1997**,*144.6,* 2045-2052.

22. O. Mao, R.A. Dunlap, J.R. Dahn. Mechanically alloyed Sn-Fe (-C) powders as anode materials for Li-Ion batteries: I. the Sn_2Fe-C system. *J. Electrochem. Soc.* **1999,** *146,* 405

23. C.-M. Park, H.-J. Sohn. A mechano-and electrochemically controlled SnSb/C nanocomposite for rechargeable Li-ion batteries. *Electrochim. Acta.* **2009***, 54,* 6367–6373

24. M. Wachtler, M. Winter, J.O. Besenhard. Anodic materials for rechargeable Li-batteries. *J. Power Sources.* **2002,** *105,* 151

25. H. Li, Q. Wang, L. Shi, L. Chen, X. Huang. Nano-alloy anode for lithium ion batteries. *Chem. Mater.* **2002,** *14,* 103

26. J. Yang, Y. Takeda, N. Imanishi, J.Y. Xie, O. Yamamoto. Intermetallic $SnSb_x$ compounds for lithium insertion hosts. *Solid State Ionics.* **2000,** *133,* 189

27. C.Q. Zhang, J.P. Tu, X.H. Huang, Y.F. Yuan, S.F. Wang, F. Mao Preparation and electrochemical performances of nanoscale $FeSn_2$ as anode material for lithium ion batteries. *J Alloys Compd.* **2008,** *457,* 81–85

28. J. Yin, M. Wada, S. Yoshida, K. Ishihara, S. Tanase, T. Sakaia. New Ag-Sn alloy anode materials for lithium-ion batteries. *J. Electrochem.* **Soc. 2003,** *150,* A1129.

29. Aifantis, K. E.; Hackney, S. A.; Dempsey, J. P. Design Criteria for Nanostructured Li-Ion Batteries. *J. Power Sources.* **2007,** *165,* 874-879.

30. Yoshio, Masaki, et al. Effect of Carbon Coating on Electrochemical Performance of Treated Natural Graphite as Lithium-Ion Battery Anode Material. *Journal of The Electrochemical Society* **2000** *147.4*, 1245-1250.

31. Min-Sik Park, Scott A. Needham, Guo-Xiu Wang, Yong-Mook Kang, Jin-Soo Park, Shi-Xue Dou, Hua-Kun Liu. Nanostructured SnSb/Carbon Nanotube Composites Synthesized by Reductive Precipitation for Lithium-Ion Batteries. *Chemistry of Materials.* **2007,** *19,* 2406-2410

32. Yadav, Thakur Prasad, Ram Manohar Yadav, and Dinesh Pratap Singh. Mechanical milling: a top down approach for the synthesis of nanomaterials and nanocomposites. *Nanoscience and Nanotechnology.* **2012,** *2.3,* 22-48.

33. A. D. W. Todd, R. E. Marr, and J. R. Dahn. Combinatorial Study of Tin-Transition Metal Alloys as Negative Electrodes for Lithium-Ion Batteries. *J. Electrochem. Soc.* **2006,** *153,* A1998-A2005;